Engineering fluorescent reporters in human pluripotent cells and strategies for live imaging human neurogenesis

Alwyn Dady*[1], Lindsay Davidson, Nicolas Loyer, Sophie Rappich[2], Greg Findlay[2], Timothy Sanders[3], Jens Januschke & Kate G. Storey*

Division of Molecular, Cell & Developmental Biology, School of Life Sciences, University of Dundee, Dundee DD1 5EH, UK

* co-corresponding authors

[1] Current position: Université Paris Est Créteil (UPEC), Glycobiology, Cell Growth and Tissue Repair Research Unit (Gly-CRRET), F-94010 Créteil, France

[2]MRC-PPU, School of School of Life Sciences, University of Dundee,

[3]University of California, San Francisco, Benioff Children's Hospital Oakland, USA

Running title: human PSC reporters for live imaging

Key words: human pluripotent cells, human spinal cord development, human cortical development, live cell imaging, piggyBac-mediated fluorescent reporters

Abstract

Investigation of cell behaviour and cell biological processes underlying human development is facilitated by creation of fluorescent reporters in human pluripotent stem cells, which can be differentiated into cell types of choice. Here we report use of a piggyBac transposon-mediated stable integration strategy to engineer human pluripotent stem cell reporter lines. These express a plasma membrane localised protein tagged with the fluorescent proteins eGFP or mKate2, the photoconvertible nuclear marker H2B-mEos3.2, or the cytoskeletal protein F-tractin tagged with mKate2. Focussing on neural development these lines were used to live image and quantify cell behaviours, including cell cycle progression and cell division orientation in spinal cord rosettes. Further, lipofection-mediated introduction of piggyBac constructs into human neural progenitors labelled single cells and small cell groups within rosettes, allowing individual cell behaviours including neuronal delamination to be monitored. Finally, using the F-tractin-mKate2 hiPSC line, novel actin dynamics were captured during proliferation in cortical neural rosettes. This study presents and validates new tools and techniques with which to interrogate human cell behaviour and cell biology using live imaging approaches.

Introduction

Live imaging is used to monitor cell behaviour within tissues and to reveal sub-cellular protein dynamics. This includes important cellular processes such as cell cycle progression and changes in cell shape and adhesion as cells differentiate and tissues form. Such observations provide insight into developmental and tissue homeostasis mechanisms and can elucidate disease cell states. The ability to genetically engineer human pluripotent stem cells to express fluorescent proteins facilitates live imaging approaches and allows high resolution investigation of cell behaviour and cell biological processes in human tissue models.

Here we create a series of human pluripotent stem cell reporter lines for live cell imaging using the non-viral plasmid based piggyBac transposon system to introduce fluorescent proteins that localise to a range of subcellular compartments (Ding, et al., 2005, Woodard and Wilson, 2015). This approach involves cloning a sequence of interest into a transposon plasmid so that it is flanked by Inverted Terminal Repeat (ITR) sequences (Figs 1A,B), which allow the piggyBac transposase to then cut and paste the sequence within TTAA-chromosomal sites distributed across the genome (Chen, et al., 2020, Elick, et al., 1996, Lee, et al., 2011, Liu, et al., 2013). Large (Li, et al., 2011) and multiplexed sequences (Kahlig, et al., 2010, Moriarity, et al., 2013) can be introduced, and can also be cleanly excised (Elick, et al., 1996), facilitating cell reprogramming approaches (Woltjen, et al., 2009, Yusa, et al., 2009). The piggyBac transposon system is particularly advantageous for live-cell imaging as it can deliver multiple transgene copies, ranging from 1-10 per haploid genome determined by titration of transposase to transposon ratios (Doherty, et al., 2012). Moreover, different transposases exhibit distinct transduction efficiencies, with hyperactive piggyBac transposase (HyPBase) providing more stable gene expression than native piggyBac or the Tc1/*mariner* transposase *Sleeping Beauty* (Doherty, et al., 2012, Yusa, et al., 2011).

The robust expression delivered by use of HyPBase may help to ensure good detection sensitivity for fluorescent proteins, in turn reducing imaging exposure times and so potential phototoxicity. This can be further combined with FACS to select moderate expression levels and so minimise potential interference with protein function. Moreover, the transposon system obviates drawbacks of directly engineering endogenous proteins (e.g. using site specific nucleases, TALENS, (Hockemeyer, et al., 2011, Joung and Sander, 2013, Miller, et al., 2011, Wood, et al., 2011) or CRISPR/Cas9, (Charpentier and Doudna, 2013, Doudna and Charpentier, 2014, Jinek, et al., 2012, Pacesa, et al., 2024), which rely on sufficient endogenous promoter strength for fluorescence detection and risk dysfunction of fluorescently tagged endogenous proteins (Roberts, et al., 2017).

Here we use HyPBase to create human pluripotent stem cell reporter lines (or to introduce constructs into cells in *in vitro* generated human tissue), which express fluorescent proteins that localise to the plasma-membrane, chromatin, or actin cytoskeleton. We characterise these lines and

113 transduced tissues and deploy innovative live imaging protocols to capture fundamental characteristics
114 of human neuroepithelial cell behaviour. These tools and approaches allowed analysis of cellular and
115 sub-cellular dynamics during cell cycle progression, including inter-kinetic nuclear migration
116 (IKNM)(Sauer, 1935, Spear and Erickson, 2012) and cell delamination in developing spinal cord, as well
117 as novel F-actin dynamics at the cell membrane and nuclear envelope in cerebral cortex.
118

119 ## Results and Discussion

120

121 ### Generation of human pluripotent cell fluorescent reporter lines using the piggyBac-transposon stable
122 integration system

123 To facilitate analysis of cell behaviour in live tissue derived from human pluripotent stem cells we
124 generated a series of fluorescent reporter hESC or iPSC lines (Dady, et al., 2022) (Figs 1A,B). To monitor
125 cell shape and dynamics we used a plasma membrane (pm) localised protein tagged with eGFP or
126 mKate2 (pm-eGFP or pm-mKate2). To allow monitoring of the cell nucleus we engineered a line
127 expressing H2B-mEos3.2, the latter localising in the nucleus and mEos3.2 having the potential for laser-
128 mediated photo-conversion (Zhang, et al., 2012) and so labelling and tracking of individually selected
129 cells. This would allow clonal analysis in combination with immunofluorescence for cell type specific
130 marker proteins. We also co-transfected H2B-mEos3.2 and pm-mKate2 expressing plasmids to allow
131 monitoring of labelled nuclei and changes in cell shape. Finally, to observe actin cytoskeletal dynamics
132 we selected F-tractin, for its minimal impact on cytoskeletal homeostasis (Belin, et al., 2014), and
133 created an F-tractin-mKate2 cell line.

134 These reporters were generated using the hESC line H9 (for pm-eGFP, pm-mKate2, H2B-
135 mEos3.2), or hiPSC line ChiPS4 for F-Tractin-mKate2 and a further pm-eGFP line (Dady, et al., 2022) and
136 we deployed the piggyBac transposon-mediated stable integration strategy (Sanders, et al., 2013,
137 Sarkar, et al., 2003, Yusa, et al., 2009, Yusa, et al., 2011). The piggyBac vectors include the fusion protein
138 of interest driven by a CAG promoter. This cargo is then flanked by two Inverted Terminal Repeat (ITR)
139 sequences which allow a hyperactive piggyBac transposase HyPBase to cut and paste cargo within
140 TTAA-chromosomal sites (Figs 1A,B).

141 The cloning strategy for generating the reporter constructs is described in the Methods and
142 see (Sanders, et al., 2013). Once complete these were introduced with HyPBase to a suspension of
143 hPSCs by electroporation: we determined that transfection of 5 times more piggyBac vector than
144 transposase was critical for efficient stable integration (Figs 1C,D) and see Methods. hPSCs transfected
145 with fusion constructs of interest were then FAC-sorted using their specific fluorescence properties
146 (Fig. S1) to generate polyclonal cell lines selected for expression of easily detectable (medium level)
147 fluorescence for live imaging studies. Single cells could then be selected to make clonal lines that would

148 obviate the potential for cell-to-cell variation to impact cell behaviours captured in live imaging
149 experiments: this was done for pm-eGFP in ChiPS4 (Fig. 1D).
150
151 **Using human pluripotent cell fluorescent reporter lines to monitor and quantify cell behaviour in**
152 **human spinal cord rosettes**
153 These fluorescent reporter hPSC lines allowed the development of *in vitro* assays for monitoring and
154 quantifying human cell behaviour. Here we first focussed on capturing fundamental parameters of
155 human neurogenesis using our established spinal cord rosette assay (Fig. 2A) (Dady, et al., 2022, Verrier,
156 et al., 2018). This involves differentiating hPSCs into Neuro-Mesodermal Progenitor-like cells (NMP-like
157 cells) and subsequently into SOX2-expressing neural progenitors, which self-organise into neural
158 rosettes exhibiting localised expression of apico-basal polarity markers such as NCAD/CDH2 by Day 6
159 (D6) following NMP-L cell plating (Fig. 2A). This differentiation assay generates neural crest and dorsal
160 neural progenitors, with the first neurons apparent from D8, peak neurogenesis at D14 and gliogenesis
161 onset by ~ D20 (Dady, et al., 2022). This sequence of events aligns with those documented in human
162 embryonic spinal cord with dorsal neurogenesis at forelimb level commencing by CS12/13 and
163 gliogenesis by CS18 (Dady, et al., 2022, Rayon, et al., 2020).
164 We set out to monitor neuroepithelial cell behaviour as cells progressed through the cell cycle
165 during IKNM(Sauer, 1935, Spear and Erickson, 2012). This behaviour is characteristic of pseudo-
166 stratified epithelia and involves movement of the nucleus from the basal to the apical side of a cell in
167 G2 phase, subsequent mitosis at the apical (ventricular) surface and return to the basal surface in G1:
168 here a neuroepithelial cell may then either re-enter S-phase or exit the cell cycle and commence
169 neuronal differentiation. To observe IKNM in spinal cord rosettes we first optimised our assay to
170 address a challenge of longer-term live imaging, increasing thickness of the developing tissue over time
171 (D6 rosettes are typically ~ 100µm thick). This reduces the ability to maintain cells of interest in focus,
172 even when deploying a long working-distance lens and deconvolution algorithms. To reduce the rosette
173 thickness we developed a re-plating regime in which D6 rosettes were manually micro-dissected and
174 replated on glass-bottom dishes suitable for microscopy (Fig. 2B). This resulted in formation of small
175 satellite micro-rosettes (SmR) surrounding the replated primary rosette (PrR) (Fig. 2C). Satellite micro-
176 rosettes were polarised as indicated by apical actin localisation. Most importantly, SmR were flatter (~
177 50µm thick) allowing longer term high-resolution live cell imaging.
178 Human spinal cord satellite rosette cells derived from hESCs expressing pm-eGFP or co-
179 expressing pm-mKate and H2B-mEos3.2 were then imaged at 10min intervals for 24h at D13-D14 and
180 D18-D19 (Figs. 2D-E, Movie 1). Apical visiting time (defined as the period during which a basally located
181 nucleus transits to the apical surface, divides and returns to a basal position) was used as an indication
182 of changing cell cycle duration: this period increased from D13-D14 to D18-D19, ~doubling over this 6-

183 day period (D13, 11h ± 3h; D19, 25h ± 7h (Fig. 2F). This real time measurement confirmed that cell cycle
184 extends as hESC-derived spinal cord progenitors age (Rayon, et al., 2020). These findings further
185 correlate with studies in mouse (Calegari, et al., 2005, Calegari and Huttner, 2003, Takahashi, et al.,
186 1995), and chick (Olivera-Martinez, et al., 2014) embryos showing that neuron-generating divisions,
187 which appear later in development, are characterized by longer IKNM and cell cycle.
188

189 **Labelling and live-imaging individual human spinal cord rosette cells using temporally defined**
190 **lipofection of piggyBac constructs**

191 We further wished to monitor sub-cellular behaviour within the developing neuroepithelium. To
192 achieve this, we devised a strategy to target a mosaic of cells in established neural rosettes using
193 lipofection. PiggyBac constructs and HyPBase transposase were transfected into D8/D9 human spinal
194 cord neural progenitors using lipofectamine (Felgner, et al., 1987)(Fig. 3A). Following further
195 differentiation this approach labelled single cells or small cell groups within rosettes (Figs.3 B,C).
196 Lipofection of cells with pm-mKate and H2B-mEos3.2 plasmids revealed cell shape and
197 chromatin configuration and so facilitated analysis of cell division and mitotic spindle orientation.
198 Rosettes containing such cells were cultured from D8/D9 to D13 or D18 and imaged at 10 min intervals
199 for 24-30h. Most divisions between D13 and D14 had vertical cleavage planes, while between D18 and
200 D19 most divisions exhibited horizontal cleavage planes: consistent with a change from neural
201 progenitor cell population expansion to the generation of daughter cells with different, asymmetric,
202 cell fates, such as a neuron and a progenitor (Casas Gimeno and Paridaen, 2022)(Figs 3D-F, Movie 3).
203 These findings demonstrate that division orientation alters as development proceeds in human spinal
204 cord neuroepithelium. This change correlates with the longer apical visiting times observed above and
205 the accumulation of neurons in later stage human spinal cord rosettes (Dady, et al., 2022). To monitor
206 delamination of new-born neurons within rosettes we followed individual cells with a basally located
207 nucleus and a long cellular process inserted into the apical rosette surface. A subset of cells underwent
208 delamination and exhibited abscission of an apical membrane particle in a manner characteristic of the
209 apical abscission mechanism first found in the chicken (Das and Storey, 2014, Kasioulis, et al.,
210 2017)(Figs. 3G, 3H and Movie 5).
211 Overall, these analyses confirm that expansion of early human spinal cord progenitors is
212 followed by slower cell cycle progression, increased asymmetric cell division and the generation of
213 neurons, and reveal conservation of apical abscission during human neuronal delamination. These
214 findings demonstrate that normal neuroepithelial cell behaviours can be captured using this piggyBac
215 engineering approach to introduce fluorescent reporters.
216

217 Live imaging F-tractin uncovers novel actin dynamics in cortical rosettes

218 Filamentous actin is a fundamental cytoskeletal component involved in the mechanics of cell division,
219 motility and force transduction within tissues (Davidson and Cadot, 2021, Gunasekaran, et al., 2022,
220 Hyrskyluoto and Vartiainen, 2020), and recent work has identified cell type and cell state specific
221 nuclear roles, e.g. (Okuno, et al., 2020). Within the developing vertebrate neuroepithelium actin
222 mediates IKNM (Norden, et al., 2009, Spear and Erickson, 2012, Yanakieva, et al., 2019) cell adhesion
223 and cell delamination, e.g. (Das and Storey, 2014, Kasioulis, et al., 2017) and intercellular filopodial
224 contacts (Zhang and Scholpp, 2019). Actin dysfunction in human cerebral cortex leads to periventricular
225 heterotopia (Sheen, et al., 2005): it disrupts cell adhesion, proliferation and neuronal delamination and
226 is associated with seizures, dyslexia and psychiatric disorders (Lian and Sheen, 2015). Moreover, the
227 uniquely human fusion gene *CHRFAM7A* acts in part by activating actin in neuronal progenitors,
228 impacting growth cone extension, dendritic spine formation and synaptic clustering (Szigeti, et al.,
229 2023). The mechanisms by which actin regulates such critical processes in the developing human brain
230 have yet to be elucidated.

231 To analyse actin dynamics, we first established cerebral cortex (cortical) neural rosettes
232 following a dual-SMAD forebrain differentiation protocol after (Chambers, et al., 2009), and rosette
233 structures were generated by D18 (Fig. 4A). Cortical rosettes made with the ChiPS4 parental line and
234 the F-tractin-mKate2 hiPSC line were characterised at D29 for expression of neural progenitor and
235 neuronal markers, and included a few TBR2/EOMES positive cells indicative of forebrain basal
236 progenitors (Figs S2A-D)(detection of TBR2/EOMES was further confirmed in cortical rosettes
237 differentiated with the Wnt signalling antagonist XAV939 Fig.S2E). The F-tractin-mKate2 hiPSC line was
238 then used to investigate actin localisation in fixed tissue and by live-cell imaging using laser-scanning
239 confocal microscopy (D28-29). F-tractin was detected in the neural progenitor cell cortex and was
240 enriched at apical cell junctions and in rounding mitotic cells within rosettes; with similar localisation
241 patterns revealed by phalloidin staining in both the parental ChiPS4 line and F-tractin-mKate2 hiPSC
242 line-derived cortical rosettes (Figs.4B,4C, Movie 4).

243 In movies, apical F-Tractin enrichment was also observed during cell delamination (Fig 4D,
244 Movie 5). Low-level F-Tractin was detected in the cytoplasm but not in the nucleus (Figs 4C-E). Most
245 divisions (97%) took place at the apical surface, with the vast majority (91%) exhibiting a vertical (Fig.
246 4E, Movie 6) and remaining divisions (9%) a horizontal cleavage plane (Fig. 4F, Movie 7). A small number
247 of basal divisions within the plane of rosettes (Fig.S3, Movie 8) correlated with the few TBR2-expressing
248 cells at this time (Figs.S2A, S2C). Interestingly, during prophase of mitosis, novel F-Tractin was enriched
249 at the basal nuclear membrane prior to Nuclear Envelope Breakdown (NEB) (Figs 4E-G). Actin
250 polymerises around the entire nuclear envelope in mitotic U2OS human cells prior to NEB and
251 associates with nuclear envelope remnants to facilitate chromosome congression and correct

252 segregation (Booth, et al., 2019). This novel actin polymerisation at the basal nuclear surface in cortical
253 progenitors may act similarly, but here act to prevent basal chromosome displacement and so enable
254 apically localised mitosis during IKNM. Following NEB, strong enrichment of F-Tractin was then
255 observed in the basal cell-cortex as the nucleus moved apically and ceased with cell rounding (Figs 4E,
256 4F). A thin basal process then persisted (Fig 4E, 26') prior to cytokinesis. Overall, these data reveal
257 established and novel actin localisations and dynamics in human cortical progenitors.
258
259 This study demonstrates the use of the HyPBase piggyBac transposase to generate fluorescent
260 protein reporters in human pluripotent cell lines. Efficient stable integration and moderate expression
261 levels were achieved by optimising, i) the quantity and ratio of piggyBac plasmids and transposase and
262 ii) subsequent FACS to exclude high expressing cells, as well as iii) transfection methods, including
263 temporally defined lipofection in hiPSC-derived tissues. The piggyBac system inserts randomly at TTAA
264 sites typically in open chromatin and so is vulnerable to construct silencing during chromatin re-
265 organisation as hiPSCs differentiate. This was mitigated here by use of polyclonal lines and we did not
266 observe silencing in our neural tissue assays, but differentiation for longer periods and into other cell
267 types might lead to loss of expression particularly in clonal lines. Despite this, these approaches will be
268 valuable for cell biological investigation of early differentiation of other cell types from hiPSCs, more
269 sophisticated neural organoids, and explanted tissues. Such assays could be used to investigate
270 environmental stressors (such as toxins or extreme heat) on human cell behaviour. The ability to
271 visualise the actin cytoskeleton and other cell biological components may also facilitate biomechanical
272 studies in human tissues. These reporter cell lines could be further used in pharmacological studies,
273 chemical genetics approaches or functional assays involving acute targeted degradation of proteins
274 using proteolysis targeting chimeras (PROTACs) to elucidate molecular mechanisms underlying
275 fundamental cellular and developmental processes.

Materials and Methods

Human pluripotent cell authentication and quality control

Human ESC line H9 was obtained from WiCell and human iPSC line ChiPS4 from Cellartis AB, now Takara Bio Europe. These suppliers provided documentation confirming cell identity. STR DNA profiling for ChiPS4 and ChiPS4-pmGFP (polyclonal), H9 (WA09) confirmed identity of these lines in our laboratory. All cell lines were expanded and banked on arrival. Prior to experiments representative lots of each cell bank were thawed and tested for post-thaw viability and to ensure sterility and absence of mycoplasma contamination. Sterility testing was performed by direct inoculation of conditioned medium into tryptic soya broth and soya bean casein broth and no contamination was observed. Mycoplasma testing was carried out by DAPI staining of fixed cultures and using the mycoalert mycoplasma detection kit (Lonza). We confirm that the cell lines used in this study were free of mycoplasma and aerobic bacteria and fungi.

H9 (WA09) hES cells were supplied at passage 24, the cells were thawed, and cell banks prepared at passage 29: for experiments the cells were used between passage 31 and 41. ChiPS4 hiPS cells were supplied at passage 9 and cell banks prepared at passage 13: for experiments the cells were used between passage 15 and 25. Two passages after thawing cells were checked for uniform expression of pluripotency markers (OCT4, SOX2, NANOG, SSEA-3, SSEA-4 TRA-1-60 and TRA-1-81), absence of differentiation markers (SSEA-1, HNF3-beta, beta-III-tubulin and smooth muscle alpha actinin) by immunofluorescence (details below).

Human pluripotent cell culture

Human pluripotent stem cells were maintained as feeder-free cultures in TESR medium (Ludwig, et al., 2006) supplemented with bFGF (30ng/mL, Peprotech) and Noggin (10ng/ml, Peprotech) on Geltrex matrix coated plates (10 $\mu g/cm^2$, Life Technologies) at 37°C in a humidified atmosphere of 5% CO_2 in air. Cells were enzymatically dispersed twice a week using TrypLE select (Life Technologies), counted using a hemacytometer and seeded on Geltrex coated plates at a density of 3e4-5e4 cells/cm^2. For single-cell passaging, the medium was supplemented by addition of the Rho kinase inhibitor Y-27632 (10 μM, Tocris). All work with hESCs was undertaken in accordance with the UK Stem Cell Bank steering committee guidance (license number SCSC14-29).

Plasmid expression constructs

The APX1 (**A**dvanced **P**iggyBac E**x**pression) plasmid was synthetically engineered to harbor improved PiggyBac inverted terminal repeats (ITRs), the cytomegalovirus (CMV) enhancer/chicken Beta-actin (CAG) promoter, woodchuck (hepatitis virus) post regulatory element (WPRE), which increases

312 transgene expression (Higashimoto, et al., 2007), and the Life Technologies Gateway recombination
313 cassette allowing for efficient phiC31-mediated recombination (Sanders, et al., 2013)(Figure 1A).
314 Subcellularly localized fluorescent protein gene cassettes were synthesized by overlap extension PCR
315 and cloned into the Gateway Entry Vector, pENTRDTOPO, and sequence verified. High efficiency
316 transposase-mediated insertion of the PiggyBac transposon cassette was accomplished through
317 transient co-expression of the mammalian optimized PiggyBac transposase (CMV HyPBase, (Yusa, et al.,
318 2011)).
319
320 For multicolour labelling of subcellular structures, we utilized monomeric enhanced green fluorescent
321 protein (mEGFP) (gift from Karel Svoboda, Addgene plasmid #18696) (Harvey, et al., 2008) and far-red
322 mKate2 (Evrogen). These proteins were selected for their photostability, low toxicity, high brightness
323 and distinct emission spectra for dual-colour assays making them suitable for live-cell imaging. To label
324 the outer leaflet of the cell membrane, membrane-associated palmitoylated proteins were generated
325 by appending 20-amino acid sequence of ratGAP-43 (MLCCMRRTKQVEKNDEDQKI) to the N-terminus
326 (pm-XFP). To label the cell nucleus, mEos3.2, a green-to-red photoconvertible protein (a gift from
327 Michael Davidson & Tao Xu (Addgene plasmid 54525), was coupled to Histone 2B (H2B) (Zhang, et al.,
328 2012). For labeling of filamentous actin, F-Tractin which contains the inositol triphosphate 3-kinase
329 actin binding domain (Belin, et al., 2014) was coupled to mKate2. Cell lines expressing both H2B-
330 mEos3.2 and pm-mKate2 were then created by co-transfection of each construct and selection for dual
331 expressing cells using FACS.
332
333 hPSCs transfection
334 H9 hESCs or hIPSCs were transfected using a Neon electroporator using 10 μl tips (Life Technologies).
335 Briefly, cells were dispersed, resuspended in TESR medium and counted as described above. For each
336 transfection 1e6 cells were collected by centrifugation at 300 xg for 2 minutes, washed with 1ml of PBS,
337 then resuspended with 10μl of Neon electroporation buffer R. 1μg of piggyBac vector and 0.2μg of
338 CMV HyPBase vector was then added to the cells in a volume of 2μl. The cells were then electroporated
339 (1150v, 30 mSec, 1 pulse), resuspended in TESR medium supplemented with bFGF, Noggin and Y27632
340 and plated on Geltrex coated dishes. Cells were maintained as described above then FAC-sorted 10
341 days after transfection.
342
343 Flow cytometry and cell sorting
344 Transfected hESCs or hiPSCs were dispersed and re-suspended as described above, then sorted by FACS
345 using a SH800 (Sony) cell sorter as a bulk pool of cells with a narrow gate selected for robustly
346 expressing cells. Quadrant gates used to estimate the percentage of positive cells and level of

347 fluorescence needed were designed based on fluorescence levels detected in the non-transfected
348 control samples. Sorted cells expressing medium levels of fluorescence were expanded and frozen then
349 representative lots of each polyclonal cell line were thawed and tested for mycoplasma contamination
350 using the MycoAlert assay (Lonza), and fungi and aerobic bacteria sterility by inoculating conditioned
351 medium into trypticase soya broth (Sigma Aldrich). No contamination was observed. In some instances
352 (pm-eGFP in ChiPSC4) monoclonal cell lines were made from the polyclonal FACS sorted pools. To make
353 monoclonal cell lines, 400 cells were seeded into 60 mm dishes and cultured until the colonies were 2
354 – 3 mm in diameter. They were then picked using 3.2 mm cloning discs (Sigma Aldrich) soaked in TrypLE
355 select and seeded into 96 well plates. Individual clones were then expanded in TESR medium
356 and pluripotency, including differentiation in 3 germ layers was confirmed (Supplementary data 1).
357
358 Neural differentiation assays
359 Spinal cord rosette differentiation: This was carried out following (Dady, et al., 2022, Verrier, et al.,
360 2018). Briefly, hESC were plated on Geltrex matrix (20 μg/cm2, Life Technologies) at a density of 4e4
361 cells/cm^2 in TSER medium as described and allowed to attach for 24h. Cells were differentiated for 48
362 hours in Neurobasal medium plus 1X B27, 1xN2, 1x non-essential amino acids and 1x glutamax (all
363 Thermo Fisher) (N2B27 medium) supplemented with 3 μM Chiron99021 (Tocris) and 20 ng/ml bFGF
364 (PeproTech) followed by a further 24 hours in N2B27 medium supplemented with 3 μM Chiron99021,
365 20 ng/ml bFGF, 10 μM SB431542 (Tocris) and 50 μg/ml Noggin (Peprotech) to obtain
366 NeuroMesodermal progenitors (NMPs). For neural differentiation of NMPs, these cells were then
367 passaged using PBS-EDTA 0.5mM and seeded back at controlled density (1e5 cells/cm2) on Geltrex
368 (20μg/cm2, Life Technologies) in N2B27 medium supplemented with 10 μM SB431542, 50 μg/ml
369 Noggin, 100 nM all-trans retinoic acid (Sigma Aldrich) and 10 μM Y27632 (Tocris). After 24 hours the
370 medium was removed and replaced with N2B27 medium containing 100 nM all-trans retinoic acid for
371 the remainder of the differentiation. As described previously, dorsal spinal cord neural rosettes formed
372 from D6 (Dady, et al., 2022) and medium was refreshed every 3 days.
373
374 Forebrain/Cortical rosette differentiation: hPSCs were dispersed as described above, counted, and re-
375 suspended in TESR medium supplemented with bFGF (30 ng/ml), Noggin (10 ng/ml) and Y27632 (10
376 μM) at a concentration of 1e5 cells/ml. 100 μl of cell suspension (1e4 cells) was then added to the
377 required number of wells of 96 well v-bottom plates and the cells pelleted by centrifugation at 300 xg
378 for 5 minutes to form embryoid bodies (EBs). EBs were cultured for 48 hours then collected from the
379 96 well plates using an 8-channel pipette, pooled and washed twice with DMEM/F12 medium (Gibco).
380 EBs were then resuspended in DMEM/F12 containing 20% knockout serum, 1x glutamax, 1x NEAA, 0.1
381 mM beta-mercaptoethanol (all Gibco), SB431542 (10 μM, Tocris) and LDN193189 (0.5 μM Sigma

382 Aldrich) and 50 EBs transferred to each well of a low attachment 6-well plate in 2ml of medium to begin
383 differentiation. Every 48 hours 1ml of medium was removed from each well and replaced with
384 Neurobasal (Gibco) containing 1x glutamax, 1x NEAA, 1x N2 (Gibco), 1x B27 (Gibco), SB431542 (10 μM)
385 and LDN193189 (0.5 μM). In some differentiations the Wnt signalling antagonist XAV939 (5 μM) (Tocris)
386 was included from D2 to D6 to increase induction of TBR2/EOMES expressing cells (Figs. S2E,F). On D9
387 of differentiation the EBs were recovered from the 6 well plates and replated on Geltrex coated (10
388 μg/cm2) 8 well chamber slides (Ibidi) using 10 – 15 EBs per well in Neurobasal containing 1x glutamax,
389 1x NEAA, 1x N2, 1x B27, SB431542 (10 μM) and LDN193189 (0.5 μM). The medium was refreshed every
390 48 hours until D15 of differentiation when it was changed to Neurobasal containing 1x glutamax, 1x
391 NEAA, 1x N2, 1x B27, BDNF (20 ng/ml, Peprotech) and GDNF (20 ng/ml, Peprotech). The medium was
392 then refreshed every 3 days, neural rosettes were evident from D18 of differentiation.
393
394 Labeling individual cells in human spinal cord rosettes by lipofection
395 For single cell or small cell group transfection, hESC (H9) cells differentiated into NMP-L cells (as above)
396 were replated at end of D3 and cultured for 8 to 9 days and then transfected using Lipofectamine 3000
397 kit (Thermo Fisher) following manufacturer's instructions with a combination of piggyBac plasmids (pm-
398 eGFP + HypBase or pm-mKate + H2B-mEos3.2 + HypBase) for a final concentration of 2 μg/μl of DNA
399 mix. These lipofected human neural progenitors were then cultured and imaged for the desired period.
400
401 Immunofluorescence
402 hPSCs and spinal cord neural rosettes were fixed in 1% paraformaldehyde solution overnight at 4°C.
403 Cortical rosettes were fixed in 4% formaldehyde for 30 min at room temperature. Samples were then
404 washed in PBS and permeabilized with 0.1% Triton X-100 or 0.1% Tween, 0.1% Triton-X in PBS (PBST),
405 blocked with 2% bovine serum albumin (BSA) or 5% donkey serum (as appropriate) for 2h at room
406 temperature. Primary antibodies were diluted as listed below in PBST and samples incubated overnight
407 on a rocker at 4°C. After washing in PBS, appropriate secondary antibodies conjugated to Alexa-fluor
408 488, 568 or 594 (Life Technologies) were applied for 2h at room temperature. Following further washes
409 in PBS samples were exposed to DAPI (1:1000) for 30 minutes, to visualize nuclei. F-actin cytoskeleton
410 was labeled using Phalloidin coupled with FITC fluorophore (1:1000; ThermoFisher).
411
412 Commercially available primary antibodies used to characterize cell types: OCT4 Cell Signaling
413 Technology (C30A3) rabbit mAb (1:400); SOX2 Cell Signaling Technology (D6D9) rabbit mAb (1:400) or
414 R&D Systems (Cat# AF2018, RRID:AB_355110) goat (1:250); NANOG Cell Signaling Technology (D73G4)
415 rabbit mAb (1:400); SSEA-4 Developmental Studies Hybridoma Bank (MC-813-70) mouse mAb (2μg/ml)
416 TRA-1-60 Cell Signaling Technology mouse mAb (1:200);TRA-1-81 Cell Signaling Technology mouse mAb

417 (1:200);SSEA-1 Developmental Studies Hybridoma Bank (MC-480) mouse mAb (2 μg per ml);HNF-3 beta
418 Cell Signaling Technology (D56D6) rabbit mAb (1:400) beta-III-tubulin Sigma Aldrich (SDL.3D10) mouse
419 mAb (1:800); Smooth muscle alpha actinin Developmental Studies Hybridoma Bank (1E12) mouse mAb
420 (2μg/ml); NCad, SIGMA, 1:500, SC-216; TBR2/EOMES 1:200 Abcam 23345, TUJ1, Covance Cat# MMS-
421 435P, mouse monoclonal 1:1000 or Biolegend (Cat# 801202, RRID:AB_2313773) mouse monoclonal
422 1:1000.TBR1 Abcam (ab31940), RRID:AB_2200219 rabbit pAB (1:200); mKate OriGene TA180091,
423 RRID:AB_2622285 mouse mAB (1:250).
424
425 Fluorescence images of fixed samples were taken on an EVOS Cell Imaging System (Thermo Fisher
426 Scientific) using x20 air lense, for hPSCs, on a Leica SP8 confocal for spinal cord rosettes using x20 air
427 lense, while cortical rosettes were imaged using a LEICA SP8 Stellaris confocal microscope (using x40 or
428 63x NA 1.4 oil immersion objective).
429
430 Generating satellite human spinal cord rosettes
431 From NMP cell passaging, transfected cells were cultured in N2B27 containing 100 nM RA (SIGMA) until
432 day 6 when neural rosettes were easily observable. Using a very sharp glass needle (0.29-0.31 mm)
433 (Vitrolife), neural rosettes were individually micro-dissected and gently deposited on a 35 mm glass
434 bottom petri dish (WPI) previously coated with Geltrex (20μg/cm2, Life Technologies). Micro-dissected
435 rosettes were then cultured in N2B27 containing 100nM RA (SIGMA) until the desired stage of
436 observation.
437
438 Live imaging of human neural rosettes
439 Cells in satellite rosettes formed from primary micro-dissected spinal cord rosettes or individual
440 lipofected neural progenitors within rosettes were imaged using a DeltaVision Core microscope system,
441 allowing detection of fine cellular detail at low fluorescence levels with minimal exposure time, in a
442 WeatherStation environmental chamber maintained at 37°C. The spinal cord rosette culture medium
443 was buffered with a 5% CO_2/95% air mix and maintained in a humid chamber. Images were acquired
444 using an Olympus 40x 1.30 NA objective using a Xenon light source and a CoolSnap HQ2 cooled CCD
445 camera (Photometrics). 30-40 optical sections (exposure time, 10-50 milliseconds for each channel,
446 1024x1024 pixels, 2x2 binning) spaced 1.5μm apart were imaged for each micro-satellite neural rosette
447 at 10-minute intervals for up to 36h. Images were deconvolved and maximum intensity projections of
448 Z-stacks were made using SoftWorx imaging software (Applied Precision) (Das, et al., 2012).

449 Confocal live imaging of cortical rosettes expressing F-Tractin+mKate2 was undertaken at 37°C with a
450 5% CO_2/95% air mix using a Leica SP8 Stellaris confocal microscope or a Zeiss spinning disc confocal

451 microscope with a x63 NA1.4 oil objective. Stacks of 18 slices optical z-section separated by 0.8 µm,
452 covering a 154×154×14.4 µm region were acquired over multiple positions every 310 seconds for up
453 to 24 hours. We applied a 3D gaussian blur with a sigma of 0.8x 0.8x 0.8 µm.
454
455 Quantification of cell behaviour
456 In spinal cord rosettes, apical visiting time was assessed by measuring time taken for a single labelled
457 cell located in the basal region of one spinal cord rosette (rosette periphery) to move to the apical
458 region and divide (rosette centre). To be consistent, observed rosettes were selected by their similar
459 diameter ~100-150 µm. At least 5 different cells per spinal cord rosette and at least 5 different rosettes
460 were analyzed for each time point (D13, D14, D18, 1D9).

461 Cell division plane was assessed by measuring the angle of the metaphase plate relative to the apical
462 surface at the lumen wall of the spinal rosette during cell division using Fiji tools. Cleavage plane was
463 considered horizontal when the metaphase plate was perpendicular to the axis of cell division. On the
464 contrary, cleavage plane was considered vertical when the metaphase plate formed an angle of 40-45°
465 to the axis of cell division (with one daughter cell remaining longer at the apical surface). All cells were
466 analysed in 3D. At least 5 different cells per spinal cord rosette and at least 5 different spinal cord
467 rosettes were analyzed for each time point.

468 In cortical rosettes, we measured the time between cell cycle phases in rosettes expressing F-Tractin-
469 mKate2. Nuclear Envelope Breakdown was identified as the moment when cytoplasmic F-Tractin
470 entered the position held by the nucleus during the previous timepoint. Completion of apical-to-basal
471 migration as the moment when the cell appeared rounded at the apical surface. Cytokinesis onset was
472 defined as the timepoint when the first membrane cortical contraction was detected. Cell division
473 cleavage planes were considered horizontal whenever one daughter cell appeared to have lost all
474 contact with the apical junctions immediately after the completion of cytokinesis. 1 to 21 cells were
475 analysed per rosette amounting to 113 cells in 11 rosettes imaged for 22 hours from D29-D30 were
476 analysed.

477 Statistical analysis
478 Statistical analysis for spinal cord rosettes was performed using non-parametric Mann-Whitney U test
479 for non-normally distributed data using Prism V8. Results are represented as means ± SEM or SD as
480 indicated in figures and p-values are indicated with *$p<0.05$, **$p<0.01$, *** $p<0.001$, and
481 ****$p<0.0001$.
482

Acknowledgements

The authors thank the University of Dundee Human Pluripotent Stem Cell Facility, Imaging Facility and the Flow Cytometry and Cell Sorting Facility for their contributions to this work.

Competing interests

The authors declare no competing interests.

Funding

This work was supported by a Wellcome Trust Investigator award to KGS (WT102817AIA-enhancement) and a Biotechnology and Biological Sciences Research Council grant (BB/V001353/1) to JJ. SR is supported by a Wellcome studentship co-supervised by KS and GF. Initial plasmid generation and cloning experiments were supported by a Children's Hospital of Pittsburgh of UPMC Research Advisory Committee Grant to AD. The Leica Stellaris confocal microscope was supported by Biotechnology and Biological Sciences Research Council grant BB/T017546/1 and the Leica SP8 by a Wellcome Trust Multi-User Equipment grant (WT101468).

Data availability

All relevant data can be found within the article and its supplementary information.

501 Figure Legends

502 Figure 1 Use of piggyBac to create human pluripotent cell fluorescent reporter lines

503 A) APX1 plasmid used for expression of fluorescent protein fusion constructs highlighting key elements;
504 B) fluorescent-protein reporter constructs for introduction into cells using piggyBac transposase; C)
505 transfection regime and FACS for selection of cells expressing constructs; D) Expression of reporters in
506 human pluripotent cell lines, pm-eGFP, pm-mKate2, H2B-mEos3.2, pm-mKate2+H2B-mEos or F-Tractin-
507 pm-mKate2. Scale bar 50µm.

508

509 Figure 2 Spinal cord differentiation and rosette generation for live imaging

510 A) Neural differentiation regime after (Verrier, et al., 2018) and neural rosette formation from NMPs
511 (D4-D14), nuclei labelled with DAPI (blue) and apical surface with N-Cadherin (NCAD); B) manual
512 microdissection of D6 primary neural rosettes (PrR), replating and culture to D14/15 and beyond
513 generates; C) small satellite micro-rosettes (SmR) around the PrR, suitable for live imaging; D) Satellite
514 micro-rosette made using pm-eGFP hESC line (Movie 1); E) selected frames from live imaging of SmR
515 following IKNM including mitosis; F) Apical visiting time quantification, revealing increase as
516 development progresses (5 independent experiments for each stage, 25 cells at D13-D14, 23 cells at
517 D18-19), means ± SD, p-values *p<0.05, **p<0.01, *** p<0.001, and ****p<0.0001. Scale bars 50 µm.

518

519 Figure 3 Lipofection-mediated mosaic transfection of spinal cord rosettes

520 A) Regime for lipofection-mediated introduction of piggyBac constructs into spinal cord rosette cells
521 and live-cell imaging; B,C) pm-mKate2 expression revealing individual neuroepithelial cell morphology
522 across apico-basal axis; D,E) Mosaic pm-mKate2+H2B-mEOS3.2 expression allowing live-cell imaging of
523 individual cells and measurement of division symmetry (Movie 2); and F) Percentage of vertical
524 (asymmetric) and horizontal (symmetric) cleavage plane divisions at apical surface in individual rosettes
525 during early and late neurogenesis (5 independent experiments for each stage: D13-14 (181 divisions
526 in 26 rosettes), D18-19 (163 divisions in 36 rosettes) means ± S.E.M; G,H) Live-cell imaging of apical
527 abscission in cell expressing pm-mKate+H2B-mEOS (Movie 3). Scale bars 50 µm.

528

529 Figure 4 Imaging F-Tractin dynamics in cortical rosettes

530 A) Summary steps of cortical neural rosette differentiation protocol; B) Comparison of F-actin
531 localisation revealed by Phalloidin binding in parental ChiPS4 line (18 rosettes, 1 experiment) and
532 engineered ChiPS4 line expressing F-Tractin-mKate2 (2 independent experiments, 18 rosettes)
533 (phalloidin images maximum-intensity-projections of 4 Z-stack planes at level of lumen); C) Live imaging
534 of cortical rosettes expressing F-Tractin, whole rosette monitored over 24h, note F-Tractin enrichment
535 in apical endfeet in rosette centre (arrowhead) and prominent apical mitoses (Movie 4); D) F-Tractin-

536 mKate2 enrichment at apical tip of a delaminating cell (9 cells in 30 rosettes)(Movie 5); Cleavage plane
537 of divisions assessed in (1 experiment, 113 divisions in 11 rosettes), **E)** vertical cleavage plane
538 (symmetric) division (103/113 divisions), values above arrows are average time between indicated
539 steps(Movie 6) and **F)** horizontal cleavage plane (asymmetric) division (10/113 divisions)(Movie
540 7); **G)** Neuroepithelial cell in a cortical rosette before and during Nuclear Envelope Breakdown (NEB),
541 representative of observations in 2 independent experiments. A (Apical), B (Basal), Arrowheads:
542 transient F-Tractin enrichment in: D delaminating cell tip, and E,F,G at basal nuclear surface; arrows: F-
543 Tractin-rich basal process; asterisks: daughter cells following cytokinesis. Scale bars: B), 50 µm; C), D)
544 20 µm, E), F) 10 µm, G) 5 µm.
545
546 Supplementary information
547
548 Movie legends
549 Live imaging of cell behaviour in human spinal cord rosettes
550 **Movie 1 (**Figs 2D,E)**:** nuclear apical-basal visiting in pm-eGFP-expressing spinal cord rosette
551 **Movie 2 (**Figs 3D,E): symmetric and asymmetric (final division) in spinal cord rosette following
552 lipofection-mediated mosaic expression of pm-mKate2+H2B-mEos3.2
553 **Movie 3 (**Figs 3G,H): Apical delamination of neuroepithelial cell following lipofection-mediated mosaic
554 expression of pm-mKate2+H2B-mEos3.2
555
556 Live imaging of cell behaviour in human cortical rosettes
557 **Movie 4** (Fig 4A): cell behaviour in F-Tractin-mKate2-expressing cortical rosette
558 **Movie 5** (Fig 4B): Apical delamination of cortical progenitor cell.
559 **Movie 6** (Fig 4C): Apical symmetrical division of cortical progenitor cell.
560 **Movie 7** (Fig 4D): Apical asymmetric division of cortical progenitor cell.
561 **Movie 8** (Fig 4SD): Basal cortical progenitor cell division.
562 Scale bars: 5 µm Movie 7; 10 µm, Movies 5, 6, 8 (bottom); 20 µm, Movies 4, 8 (top).
563
564 Supplementary Figures
565
566 Figure S1 - FASC data for human pluripotent cells expressing fluorescent reporters
567 (related to Figure 1)
568 FASC data for selection of human pluripotent cells expressing fluorescent reporters, showing
569 expression of eGFP in 82.82% of cells, mKate2 in 92.74% of cells, and H2B-mEos3 only in 22.75% of
570 cells, while 13.79% of cells co-expressed pm-Kate and H2B-mEos3.2.

571 Figure S2 - Characterisation of cortical rosettes
572 (related to Figure 4)
573 Immunofluorescence analysis of cortical rosettes, visualisation of nuclei with DAPI, F-actin with
574 Phalloidin or mKate antibody to detect F-tractin-mKate2, in parental hiPSC line ChiPS4, **A)** labelling
575 neural (SOX2), and basal (TBR2/EOMES) progenitors, and **B)** neurons TUJ1; in F-tractin-mKate2 line
576 labelling **C)** TBR2/EOMES, and **D)** TUJ1; in parental ChiPS4 line following protocol with XAV939, **E)**
577 TBR2/EOMES, and SOX2, **F)** TUJ1. Fifteen rosettes assessed from 1 experiment for each condition (with
578 or without XAV939) in parental ChiPS4 line, 30 rosettes from 2 independent experiments assessed F-
579 tractin-mKate2 line. Scale bars in A-F 50 µm.
580
581 Figure S3 - Basal cortical progenitor cell division
582 **A)** Basal cortical progenitor cell division (within the plane of the rosette, 1 experiment, 3 divisions in 11
583 rosettes) (movie 8). Scale bars: 20 µm (top) and 10 µm (bottom).
584
585 Figure S4 - Pluripotency confirmation of ChiPS4 clonal line pm-eGFP by immunofluorescence
586 Immunofluorescent detection of pluripotency proteins OCT4, NANOG and SOX2 in ChiPS4 clonal line
587 pm-eGFP. Nuclei labelled with DAPI. Scale bar 50µm.
588
589 Supplementary data
590 Supplementary data 1 - Pluripotency confirmation of ChiPS4 clonal line pm-eGFP by qPCR (Excel file)
591 The clonal ChiPS4 line expressing pm-GFP was quality controlled in 3 technical replicates by qPCR for
592 expression of pluripotency markers *OCT4* and *NANOG* and markers for differentiating endoderm,
593 mesoderm or ectoderm for *FOXA2*, *MSGN1*, *PAX6*. Spontaneous in vitro differentiation of embryoid
594 bodies (in the absence of bFGF) evidenced differentiation into cells representative of the 3 germ layers
595 further confirming pluripotency of this engineered cell line.
596
597
598
599

References

Belin, B. J., Goins, L. M. and Mullins, R. D. (2014). Comparative analysis of tools for live cell imaging of actin network architecture. Bioarchitecture 4, 189-202.

Booth, A. J. R., Yue, Z., Eykelenboom, J. K., Stiff, T., Luxton, G. W. G., Hochegger, H. and Tanaka, T. U. (2019). Contractile acto-myosin network on nuclear envelope remnants positions human chromosomes for mitosis. Elife 8.

Calegari, F., Haubensak, W., Haffner, C. and Huttner, W. B. (2005). Selective lengthening of the cell cycle in the neurogenic subpopulation of neural progenitor cells during mouse brain development. J Neurosci 25, 6533-6538.

Calegari, F. and Huttner, W. B. (2003). An inhibition of cyclin-dependent kinases that lengthens, but does not arrest, neuroepithelial cell cycle induces premature neurogenesis. J Cell Sci 116, 4947-4955.

Casas Gimeno, G. and Paridaen, J. (2022). The Symmetry of Neural Stem Cell and Progenitor Divisions in the Vertebrate Brain. Front Cell Dev Biol 10, 885269.

Chambers, S. M., Fasano, C. A., Papapetrou, E. P., Tomishima, M., Sadelain, M. and Studer, L. (2009). Highly efficient neural conversion of human ES and iPS cells by dual inhibition of SMAD signaling. Nat Biotechnol 27, 275-280.

Charpentier, E. and Doudna, J. A. (2013). Biotechnology: Rewriting a genome. Nature 495, 50-51.

Chen, Q., Luo, W., Veach, R. A., Hickman, A. B., Wilson, M. H. and Dyda, F. (2020). Structural basis of seamless excision and specific targeting by piggyBac transposase. Nat Commun 11, 3446.

Dady, A., Davidson, L., Halley, P. A. and Storey, K. G. (2022). Human spinal cord in vitro differentiation pace is initially maintained in heterologous embryonic environments. Elife 11.

Das, R. M. and Storey, K. G. (2014). Apical abscission alters cell polarity and dismantles the primary cilium during neurogenesis. Science 343, 200-204.

Das, R. M., Wilcock, A. C., Swedlow, J. R. and Storey, K. G. (2012). High-resolution live imaging of cell behavior in the developing neuroepithelium. Journal of visualized experiments : JoVE.

Davidson, P. M. and Cadot, B. (2021). Actin on and around the Nucleus. Trends Cell Biol 31, 211-223.

Ding, S., Wu, X., Li, G., Han, M., Zhuang, Y. and Xu, T. (2005). Efficient transposition of the piggyBac (PB) transposon in mammalian cells and mice. Cell 122, 473-483.

Doherty, J. E., Huye, L. E., Yusa, K., Zhou, L., Craig, N. L. and Wilson, M. H. (2012). Hyperactive piggyBac gene transfer in human cells and in vivo. Hum Gene Ther 23, 311-320.

Doudna, J. A. and Charpentier, E. (2014). Genome editing. The new frontier of genome engineering with CRISPR-Cas9. Science 346, 1258096.

Elick, T. A., Bauser, C. A. and Fraser, M. J. (1996). Excision of the piggyBac transposable element in vitro is a precise event that is enhanced by the expression of its encoded transposase. Genetica 98, 33-41.

Felgner, P. L., Gadek, T. R., Holm, M., Roman, R., Chan, H. W., Wenz, M., Northrop, J. P., Ringold, G. M. and Danielsen, M. (1987). Lipofection: a highly efficient, lipid-mediated DNA-transfection procedure. Proc Natl Acad Sci U S A 84, 7413-7417.

Gunasekaran, S., Miyagawa, Y. and Miyamoto, K. (2022). Actin nucleoskeleton in embryonic development and cellular differentiation. Curr Opin Cell Biol 76, 102100.

Harvey, C. D., Yasuda, R., Zhong, H. and Svoboda, K. (2008). The spread of Ras activity triggered by activation of a single dendritic spine. Science 321, 136-140.

Higashimoto, T., Urbinati, F., Perumbeti, A., Jiang, G., Zarzuela, A., Chang, L. J., Kohn, D. B. and Malik, P. (2007). The woodchuck hepatitis virus post-transcriptional regulatory element reduces readthrough transcription from retroviral vectors. Gene Ther 14, 1298-1304.

Hockemeyer, D., Wang, H., Kiani, S., Lai, C. S., Gao, Q., Cassady, J. P., Cost, G. J., Zhang, L., Santiago, Y., Miller, J. C., et al. (2011). Genetic engineering of human pluripotent cells using TALE nucleases. Nat Biotechnol 29, 731-734.

Hyrskyluoto, A. and Vartiainen, M. K. (2020). Regulation of nuclear actin dynamics in development and disease. Curr Opin Cell Biol 64, 18-24.

651 Jinek, M., Chylinski, K., Fonfara, I., Hauer, M., Doudna, J. A. and Charpentier, E. (2012). A
652 programmable dual-RNA-guided DNA endonuclease in adaptive bacterial immunity. Science 337,
653 816-821.
654 Joung, J. K. and Sander, J. D. (2013). TALENs: a widely applicable technology for targeted genome
655 editing. Nat Rev Mol Cell Biol 14, 49-55.
656 Kahlig, K. M., Saridey, S. K., Kaja, A., Daniels, M. A., George, A. L., Jr. and Wilson, M. H. (2010).
657 Multiplexed transposon-mediated stable gene transfer in human cells. Proc Natl Acad Sci U S A 107,
658 1343-1348.
659 Kasioulis, I., Das, R. M. and Storey, K. G. (2017). Inter-dependent apical microtubule and actin
660 dynamics orchestrate centrosome retention and neuronal delamination. Elife 6.
661 Lee, C. Y., Li, J. F., Liou, J. S., Charng, Y. C., Huang, Y. W. and Lee, H. J. (2011). A gene delivery system
662 for human cells mediated by both a cell-penetrating peptide and a piggyBac transposase.
663 Biomaterials 32, 6264-6276.
664 Li, M. A., Turner, D. J., Ning, Z., Yusa, K., Liang, Q., Eckert, S., Rad, L., Fitzgerald, T. W., Craig, N. L. and
665 Bradley, A. (2011). Mobilization of giant piggyBac transposons in the mouse genome. Nucleic Acids
666 Res 39, e148.
667 Lian, G. and Sheen, V. L. (2015). Cytoskeletal proteins in cortical development and disease: actin
668 associated proteins in periventricular heterotopia. Front Cell Neurosci 9, 99.
669 Liu, X., Li, N., Hu, X., Zhang, R., Li, Q., Cao, D., Liu, T., Zhang, Y. and Liu, X. (2013). Efficient production
670 of transgenic chickens based on piggyBac. Transgenic Res 22, 417-423.
671 Ludwig, T. E., Levenstein, M. E., Jones, J. M., Berggren, W. T., Mitchen, E. R., Frane, J. L., Crandall, L.
672 J., Daigh, C. A., Conard, K. R., Piekarczyk, M. S., et al. (2006). Derivation of human embryonic stem
673 cells in defined conditions. Nat Biotechnol 24, 185-187.
674 Miller, J. C., Tan, S., Qiao, G., Barlow, K. A., Wang, J., Xia, D. F., Meng, X., Paschon, D. E., Leung, E.,
675 Hinkley, S. J., et al. (2011). A TALE nuclease architecture for efficient genome editing. Nat Biotechnol
676 29, 143-148.
677 Moriarity, B. S., Rahrmann, E. P., Keng, V. W., Manlove, L. S., Beckmann, D. A., Wolf, N. K., Khurshid,
678 T., Bell, J. B. and Largaespada, D. A. (2013). Modular assembly of transposon integratable multigene
679 vectors using RecWay assembly. Nucleic Acids Res 41, e92.
680 Norden, C., Young, S., Link, B. A. and Harris, W. A. (2009). Actomyosin is the main driver of
681 interkinetic nuclear migration in the retina. Cell 138, 1195-1208.
682 Okuno, T., Li, W. Y., Hatano, Y., Takasu, A., Sakamoto, Y., Yamamoto, M., Ikeda, Z., Shindo, T.,
683 Plessner, M., Morita, K., et al. (2020). Zygotic Nuclear F-Actin Safeguards Embryonic Development.
684 Cell Rep 31, 107824.
685 Olivera-Martinez, I., Schurch, N., Li, R. A., Song, J., Halley, P. A., Das, R. M., Burt, D. W., Barton, G. J.
686 and Storey, K. G. (2014). Major transcriptome re-organisation and abrupt changes in signalling, cell
687 cycle and chromatin regulation at neural differentiation in vivo. Development 141, 3266-3276.
688 Pacesa, M., Pelea, O. and Jinek, M. (2024). Past, present, and future of CRISPR genome editing
689 technologies. Cell 187, 1076-1100.
690 Rayon, T., Stamataki, D., Perez-Carrasco, R., Garcia-Perez, L., Barrington, C., Melchionda, M., Exelby,
691 K., Lazaro, J., Tybulewicz, V. L. J., Fisher, E. M. C., et al. (2020). Species-specific pace of development
692 is associated with differences in protein stability. Science 369.
693 Sanders, T. A., Llagostera, E. and Barna, M. (2013). Specialized filopodia direct long-range transport
694 of SHH during vertebrate tissue patterning. Nature 497, 628-632.
695 Sarkar, A., Sim, C., Hong, Y. S., Hogan, J. R., Fraser, M. J., Robertson, H. M. and Collins, F. H. (2003).
696 Molecular evolutionary analysis of the widespread piggyBac transposon family and related
697 "domesticated" sequences. Mol Genet Genomics 270, 173-180.
698 Sauer, F. C. (1935). Mitosis in the neural tube. J. Comp. Neurol. 62, 377-405.
699 Sheen, V. L., Jansen, A., Chen, M. H., Parrini, E., Morgan, T., Ravenscroft, R., Ganesh, V., Underwood,
700 T., Wiley, J., Leventer, R., et al. (2005). Filamin A mutations cause periventricular heterotopia with
701 Ehlers-Danlos syndrome. Neurology 64, 254-262.

Spear, P. C. and Erickson, C. A. (2012). Interkinetic nuclear migration: a mysterious process in search of a function. Dev Growth Differ 54, 306-316.
Szigeti, K., Ihnatovych, I., Rosas, N., Dorn, R. P., Notari, E., Cortes Gomez, E., He, M., Maly, I., Prasad, S., Nimmer, E., et al. (2023). Neuronal actin cytoskeleton gain of function in the human brain. EBioMedicine 95, 104725.
Takahashi, T., Nowakowski, R. S. and Caviness, V. S., Jr. (1995). The cell cycle of the pseudostratified ventricular epithelium of the embryonic murine cerebral wall. J Neurosci 15, 6046-6057.
Verrier, L., Davidson, L., Gierlinski, M., Dady, A. and Storey, K. G. (2018). Neural differentiation, selection and transcriptomic profiling of human neuromesodermal progenitor-like cells in vitro. Development 145.
Woltjen, K., Michael, I. P., Mohseni, P., Desai, R., Mileikovsky, M., Hamalainen, R., Cowling, R., Wang, W., Liu, P., Gertsenstein, M., et al. (2009). piggyBac transposition reprograms fibroblasts to induced pluripotent stem cells. Nature 458, 766-770.
Wood, A. J., Lo, T. W., Zeitler, B., Pickle, C. S., Ralston, E. J., Lee, A. H., Amora, R., Miller, J. C., Leung, E., Meng, X., et al. (2011). Targeted genome editing across species using ZFNs and TALENs. Science 333, 307.
Woodard, L. E. and Wilson, M. H. (2015). piggyBac-ing models and new therapeutic strategies. Trends Biotechnol 33, 525-533.
Yanakieva, I., Erzberger, A., Matejcic, M., Modes, C. D. and Norden, C. (2019). Cell and tissue morphology determine actin-dependent nuclear migration mechanisms in neuroepithelia. J Cell Biol 218, 3272-3289.
Yusa, K., Rad, R., Takeda, J. and Bradley, A. (2009). Generation of transgene-free induced pluripotent mouse stem cells by the piggyBac transposon. Nat Methods 6, 363-369.
Yusa, K., Zhou, L., Li, M. A., Bradley, A. and Craig, N. L. (2011). A hyperactive piggyBac transposase for mammalian applications. Proc Natl Acad Sci U S A 108, 1531-1536.
Zhang, C. and Scholpp, S. (2019). Cytonemes in development. Curr Opin Genet Dev 57, 25-30.
Zhang, M., Chang, H., Zhang, Y., Yu, J., Wu, L., Ji, W., Chen, J., Liu, B., Lu, J., Liu, Y., et al. (2012). Rational design of true monomeric and bright photoactivatable fluorescent proteins. Nat Methods 9, 727-729.

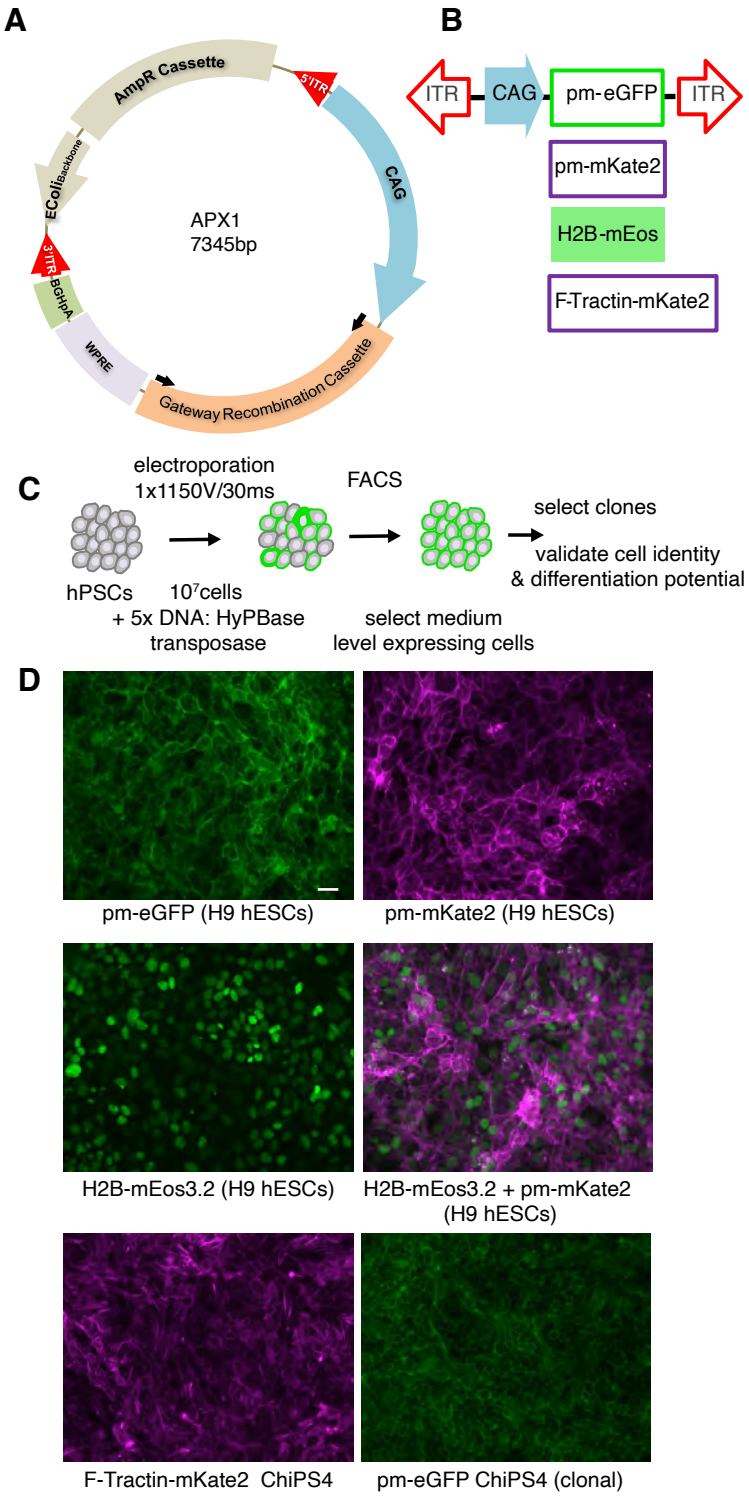

Figure 1 Dady et al

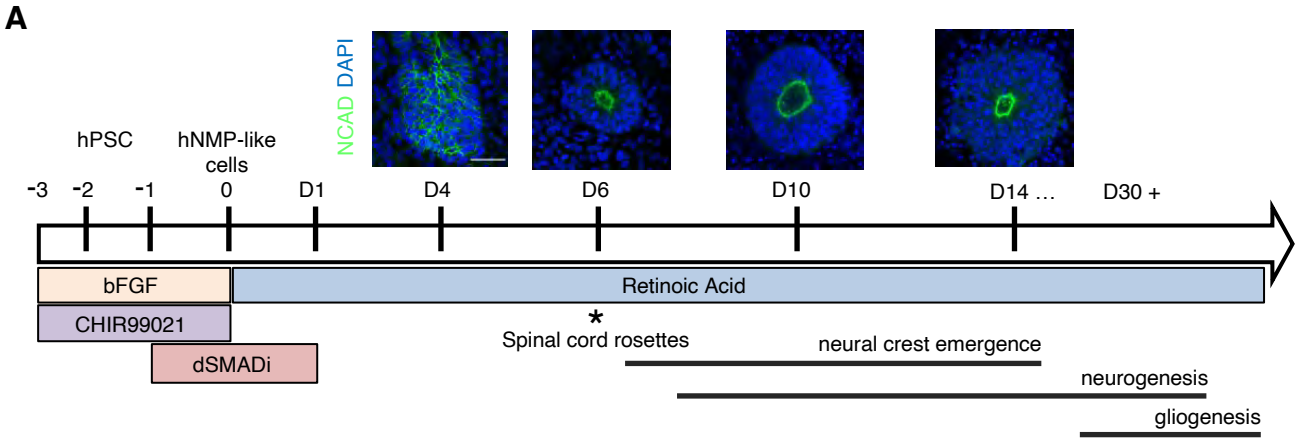

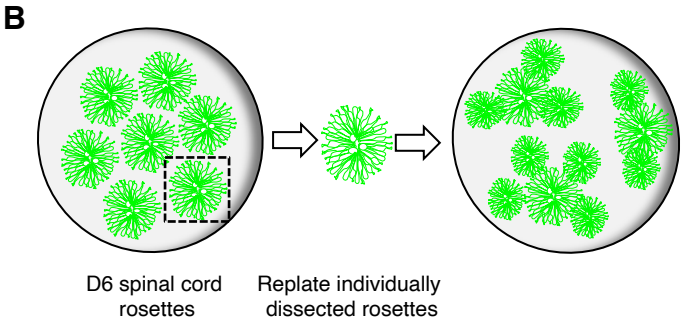

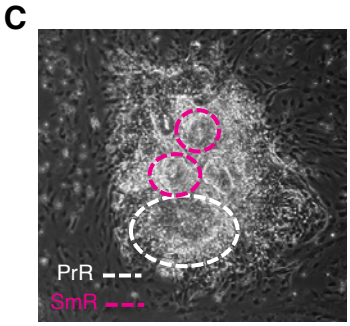

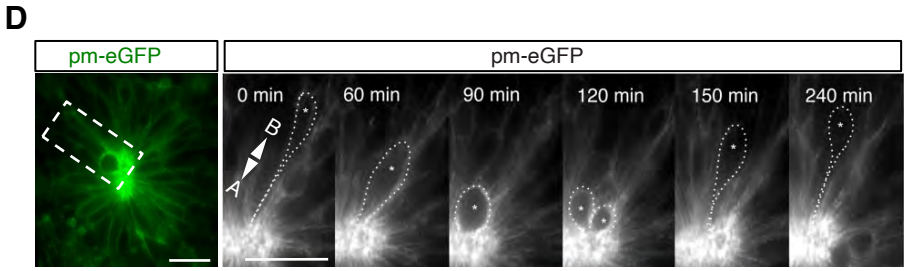

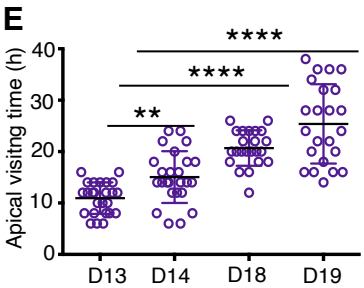

Figure 2 Dady et al

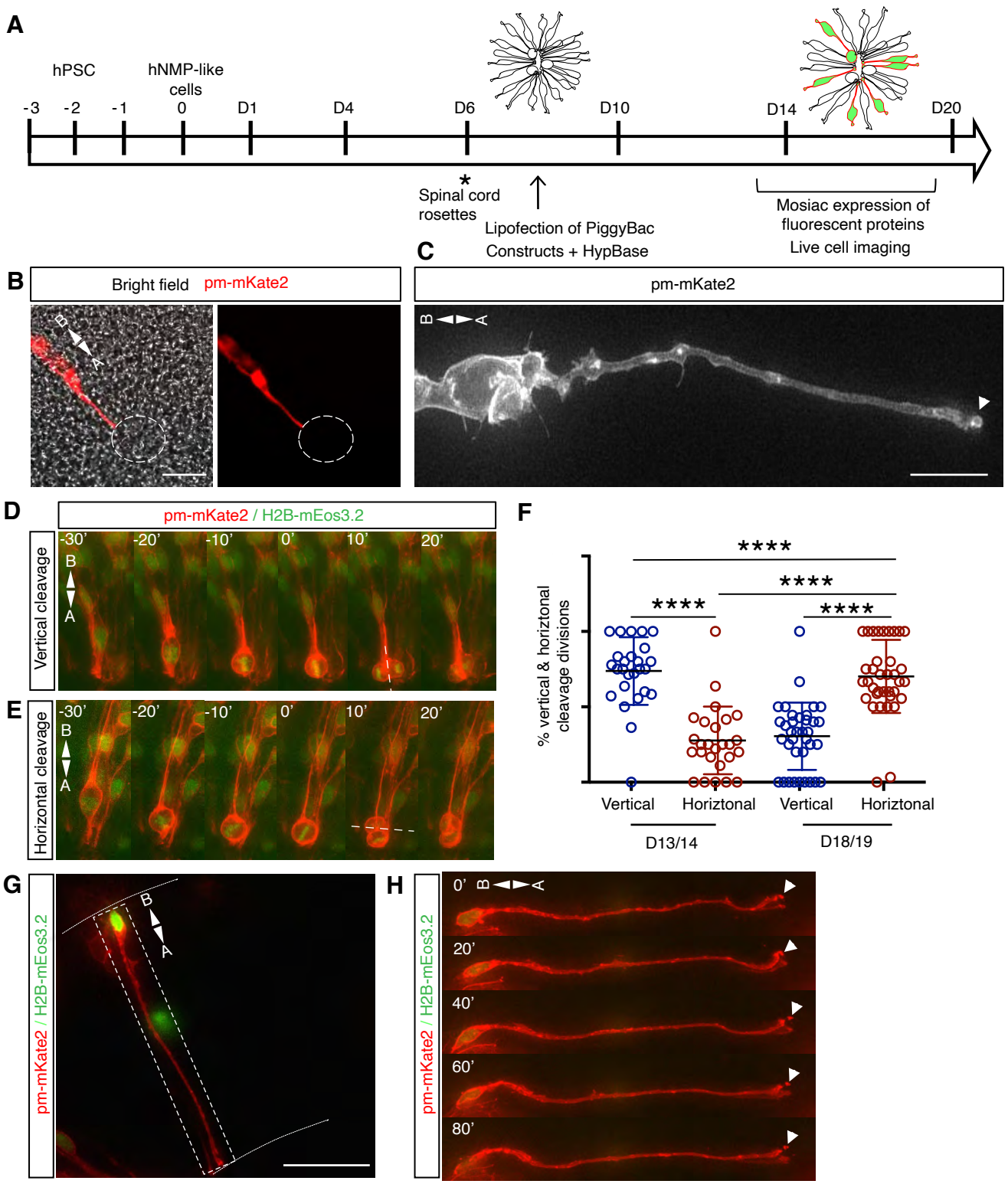

Figure 3 Dady et al

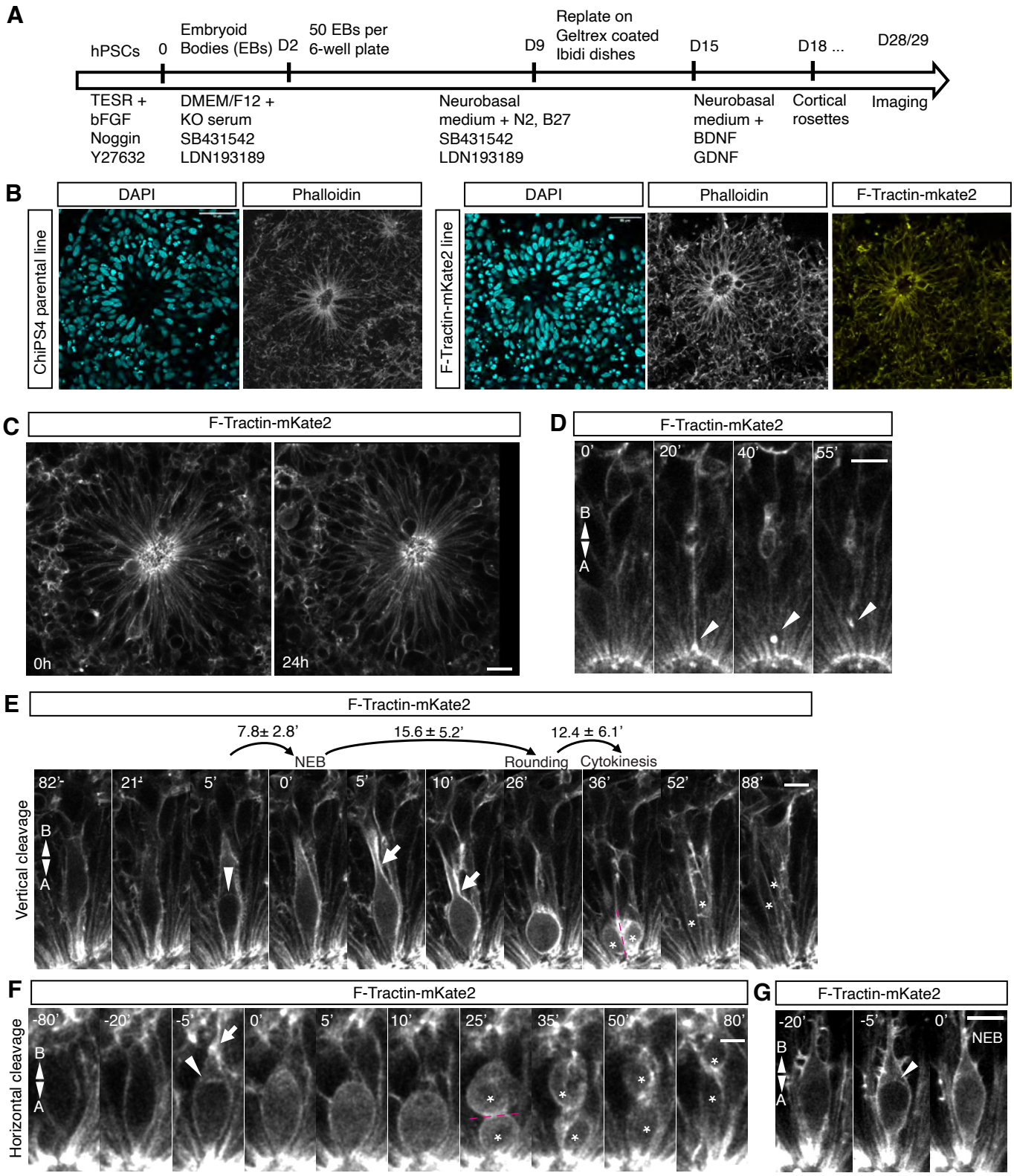

Figure 4 Dady et al